Exact static solutions to a translationally invariant discrete ϕ^4 model

Sergey V. Dmitriev[1], Panayotis G. Kevrekidis[2], Avinash Khare[3], and Avadh Saxena[4]
[1] *Institute of Industrial Science, the University of Tokyo, Komaba, Meguro-ku, Tokyo 153-8505, Japan*
[2] *Department of Mathematics and Statistics, University of Massachusetts, Amherst, MA 01003-4515, USA*
[3] *Institute of Physics, Bhubaneswar, Orissa 751005, India*
[4] *Center for Nonlinear Studies and Theoretical Division, Los Alamos National Laboratory, Los Alamos, New Mexico 87545, USA*
(Dated: February 7, 2008)

For a discrete, translationally-invariant ϕ^4 model introduced by Barashenkov *et al.* [Phys. Rev. E **72**, 35602R (2005)], we provide the momentum conservation law and demonstrate how the first integral of the static version of the discrete model can be constructed from a Jacobi elliptic function (JEF) solution. The first integral can be written in the form of a nonlinear map from which *any* static solution supported by the model can be constructed. A set of JEF solutions, including the staggered ones, is derived. We also report on the stability analysis for the static bounded solutions and exemplify the dynamical behavior of the unstable solutions. This work provides a road-map, through this illustrative example, on how to fully analyze translationally-invariant models in terms of their static problem, its first integral, their full-set of static solutions and associated conservation laws.

PACS numbers: 05.45.-a, 05.45.Yv, 63.20.-e

I. INTRODUCTION AND SETUP

In recent years, the discrete nonlinear models have played a very important role in several physics applications [1, 2]. The question of mobility of solitonic excitations in discrete media is a key issue in many physical contexts; for example the mobility of dislocations, a kind of topological solitons, is of importance in the physics of plastic deformation of metals and other crystaline bodies [3]. Similar questions arise in optics for light pulses moving in optical waveguides or in photorefractive crystal lattices (see e.g., [4] for a relevant recent discussion) and in atomic physics for Bose-Einstein condensates moving through optical lattice potentials (see e.g., [5] for a recent review). These issues may prove critical in aspects related to the guidance and manipulation of coherent, nonlinear wavepackets in solid-state, atomic and optical physics applications.

In the above settings, the translationally invariant (TI) discrete models [6] have received considerable attention since they admit static solutions that can be placed anywhere with respect to the lattice. For the Hamiltonian TI lattices [7, 8], this can be interpreted as the absence of the Peierls-Nabarro potential [3]. For the non-Hamiltonian lattices, the height of the Peierls-Nabarro barrier is path-dependent but there exists a continuous path along which the work required for a quasi-static shift of the solution along the lattice is zero [9]. In general, one can state that coherent structures in the TI models are not trapped by the lattice and they can be accelerated by even a weak external field. This particular property makes the TI discrete models potentially interesting for physical applications and one such physically meaningful model has been recently reported [10].

It has been demonstrated that some of the TI lattices support traveling solutions, but only for selected velocities [11, 12]; this feature distinguishes them from the completely integrable lattices [1, 13, 14] where the propagation velocity can change continuously. Translationally invariant discrete models can also be defined as models whose static version is exactly solvable; thus, the TI discrete models are directly connected to the theory of integrable maps [15]. Starting from the pioneering works of [6, 7], the TI discrete models have been receiving attention from several groups. General classes of such models have been constructed and investigated for the Klein-Gordon [8, 9, 10, 11, 16, 17, 18] and for the nonlinear Schrödinger equations (NLSE) [12, 19, 20, 21, 22, 23].

For a wide class of Klein-Gordon TI models it is known that they conserve momentum defined in a standard form [6] but are non-Hamiltonian. That is to say, there are TI models that conserve the standard momentum but not the standard energy. Similarly, there are models that conserve energy but do not conserve the momentum; see [16], for a detailed discussion. However, this raises the question: is there always some form of a conservation law (either as a standard momentum or a standard energy, or as a generalized version thereof) present in the TI models? In this paper, we consider an example of a model that conserves neither the standard energy, nor the standard momentum. We show in this case that a conservation of a non-standard momentum is present. The existence of a conservation law even in such a non-standard case, leads us to believe that there should always be at least one conservation law in the TI models.

It is also known that some of the discrete TI models, both of the Klein-Gordon and of the NLSE type, support exact static/stationary and sometimes even moving (with a discrete set of velocities) solutions in the form of the Jacobi elliptic functions (JEF) [8, 9, 12, 21, 22] but other TI lattices do not support JEF solutions, e.g., the lattice reported in [7].

On the other hand, for any TI lattice, the static prob-

lem can be reduced to a first-order difference equation which has been called the discretized first integral (DFI) [9, 17] because, in the continuum limit, the DFI reduces to the first integral of the static field equation. The DFI is a nonlinear map from which, for an admissible initial value, one can construct a static solution iteratively. The DFI approach can be used to construct the TI models [9, 17], but here we address the inverse problem of finding the DFI for a given TI model. We demonstrate how the DFI can be found from a known JEF solution to a TI model.

More specifically, in the present study we consider the following discrete model first suggested by Barashenkov *et al.* [18],

$$\ddot{\phi}_n = \frac{1}{h^2}\left(\phi_{n-1} - 2\phi_n + \phi_{n+1}\right) + \lambda\phi_n - \lambda\phi_{n-1}\phi_n\phi_{n+1}, \quad (1)$$

where $\lambda = \pm 1$ and overdot means derivative with respect to time. In the continuum limit ($h \to 0$) the model reduces to the ϕ^4 field theory model

$$\phi_{tt} = \phi_{xx} + \lambda\left(\phi - \phi^3\right). \quad (2)$$

The static version of Eq. (2) (with omitted inertia term ϕ_{tt}) possesses the first integral

$$\phi_x^2 - \frac{\lambda}{2}(1-\phi^2)^2 + K = 0\,, \quad (3)$$

where K is the integration constant. An exact static kink solution to the TI lattice of Eq. (1) and a two-point map that generates the kink solution were derived by Barashenkov *et al.* [18].

There are numerous reasons for the choice of Eq. (1) as our illustrative example for this study, intending to highlight the range and the power of the methods available to tackle TI models. Firstly, the model does not possess an obvious conservation law. Secondly, it does not have an obvious discrete first integral. Thirdly, its general solutions are not available and neither their parametric space, nor their stability have been explored. In the present work, we develop a number of relevant results for the lattice of Eq. (1). In particular, in Sec. II, we give (i) the corresponding conservation law; (ii) the two-point map (or DFI) from which *any* static solution of Eq. (1) can be constructed; (iii) a set of static JEF solutions. We believe that the features (i) and (ii) should be present in any TI model, and use this non-standard model to showcase how to develop them. Then, in Sec. III, we present the results of numerical studies including the stability analysis of the static solutions and, for $h^2 < 2$, we show several examples of the dynamics of unstable solutions. Section IV concludes the paper. It is worth pointing out that recently two of us [9] have similarly studied a model (henceforth called the –standard– momentum conserving or MC model)

$$\ddot{\phi}_n = \frac{1}{h^2}\left(\phi_{n-1} - 2\phi_n + \phi_{n+1}\right) + \lambda\phi_n - \frac{\lambda}{2}\phi_n^2[\phi_{n-1} + \phi_{n+1}]\,. \quad (4)$$

We shall compare and contrast the various results obtained from model of Eq. (1) with those of the MC model to get a better insight into the various issues involved.

II. ANALYTICAL RESULTS

A. Momentum conservation law

By seeking expressions that would symmetrize the form of the nonlinearity, we have found that the discrete TI model of Eq. (1) conserves the momentum defined as

$$P = \sum_n \dot{\phi}_n(\phi_{n+2} - \phi_{n-2}), \quad (5)$$

which is different from the standard definition of momentum used, e.g., in [6, 16]. The latter momentum, namely:

$$P = \sum_n \dot{\phi}_n(\phi_{n+1} - \phi_{n-1}), \quad (6)$$

is conserved e.g. by the MC model of Eq. (4). The proof in both cases is through straightforward time-differentiation and application of a telescopic summation.

B. Reduction to the first-order difference equation

It is possible to construct the first integral of the static version of Eq. (1), which can be presented in the form of the nonlinear map,

$$\begin{aligned} \phi_{n\pm1} &= (2-\Lambda)\frac{Z\phi_n \pm \sqrt{f(\phi_n)}}{2-\Lambda-\Lambda\phi_n^2}, \\ f(\phi_n) &= \frac{\Lambda}{2-\Lambda}\left(\tilde{K} - X\phi_n^2 + \phi_n^4\right), \end{aligned} \quad (7)$$

with

$$\Lambda = \lambda h^2, \quad (8)$$

$$\tilde{K} = 1 - \frac{2K}{\lambda}, \quad (9)$$

$$Z = \frac{(2-\Lambda)^2 - \tilde{K}\Lambda^2}{2(2-\Lambda)}, \quad (10)$$

$$X = \frac{\tilde{K}\Lambda^2 + (2-\Lambda)^2(1-Z^2)}{\Lambda(2-\Lambda)}. \quad (11)$$

Apart from the model parameters, h^2 and λ, the map defined by Eqs. (7) to (11) contains the integration constant K. The role of the second integration constant, for the second-order difference static equation (1), is effectively played by the initial value of the map, ϕ_0. In

Appendix I we show how the two-point map can be constructed from the known JEF solutions. Due to the symmetry of Eq. (1), in the left-hand side of Eq. (7), one can substitute $\phi_{n\pm1}$ with $\phi_{n\mp1}$.

For any pair of admissible values, K and ϕ_0, the map of Eq. (7) generates a static solution to Eq. (1). Since the same map is used for calculation of the forth and back points of the map, iterations starting from an admissible value ϕ_0 cannot give an inadmissible one and thus, the static solution will necessarily be constructed for the entire chain. From the two different roots of Eq. (7) for ϕ_{n+1} (or for ϕ_{n-1}), one should take the one different from ϕ_{n-1} (or from ϕ_{n+1}). This rule gives the sufficient condition for moving along the same solution branch and it guarantees that, for the chosen ϕ_{n+1} (or for ϕ_{n-1}), the three point problem Eq. (1) will be satisfied for ϕ_n.

In the continuum limit, the first-order difference equation (7) reduces to Eq. (3). In other words, the two-point map, as given by Eq. (7), is a DFI of the static ϕ^4 field. This observation is in line with our earlier work [9, 17] where the relation between TI discrete models and DFI of the static field equation was established.

It is interesting to note that for the MC model (4), the nonlinear map has the form [9]

$$\phi_n = \frac{(2-\Lambda)\phi_{n+1} \pm \sqrt{D}}{(2-\Lambda\phi_{n+1}^2)}\,, \tag{12}$$

where

$$D = 2\Lambda(1-\phi_{n+1}^2)^2 + 2\tilde{C}(\Lambda\phi_{n+1}^2 - 2)\,, \tag{13}$$

and $\tilde{C} = Ch^2$ with C being the integration constant.

It is also worth pointing out that while the map for the MC case given by Eqs. (12) and (13), is quadratic in both ϕ_n and ϕ_{n+1}, the map in the present case as given by Eq. (7) is, generally speaking, quartic in ϕ_n and quadratic in ϕ_{n+1}, the only exception being when $\Lambda = 2$ when the map is quadratic in both ϕ_n and ϕ_{n+1} (this is discussed in detail in Sec. II C 4). Thus, while the map in the MC case belongs to the family of twelve-parameter two-point map presented by Quispel *et al.* [15], the map in our case as given by Eq. (7) does not, in general, belong to the relevant family of maps. To be more precise, while the static version of Eq. (1) is of the Quispel *et al.* [15] form as given by

$$\phi_{n+1} = \frac{f_1(\phi_n) - f_2(\phi_n)\phi_{n-1}}{f_2(\phi_n) - f_3(\phi_n)\phi_{n-1}}\,, \tag{14}$$

with

$$f_1(\phi_n) = (2-\Lambda)\phi_n\,, \quad f_2(\phi_n) = 1\,, \quad f_3(\phi_n^2) = \Lambda\phi_n\,, \tag{15}$$

one is unable to write the corresponding invariant map in terms of the twelve parameters presented in [15].

It should however be noted that, even then, as shown below, all static solutions to Eq. (1) can be obtained iteratively from Eq. (7) with an admissible K, starting from any admissible ϕ_0.

C. Admissible values of integration constants and solutions from the nonlinear map

Throughout this paper, without any loss of generality, we will always take $\lambda = \pm 1$ and vary h so as to vary Λ.

Inadmissible values of integration constants, K and ϕ_0, are those for which, in Eq. (7), $f(\phi_0) < 0$ and $2 - \Lambda - \Lambda\phi_0^2 = 0$. For $\lambda = 1$, we need to consider separately the regime of $h^2 < 2$ (i.e. $0 < \Lambda < 2$) and the regime of very high discreteness, $h^2 > 2$ (i.e. $\Lambda > 2$). The third case is the case of $\Lambda < 0$ where, however, the topology does not change as one goes from small to large h^2. For $\Lambda = 2$ the two-point map Eq. (7) cannot be used in this form. This case is studied separately in Sec. II C 4. It may be pointed out that similar studies have already been performed for the MC model in [9].

1. *Case of* $0 < \Lambda < 2$

The inadmissible regions of the plane (K, ϕ_0) are shown by shaded areas in Fig. 1 for different values of the discreteness parameter, indicated in each panel. The topology of the admissible regions is different for $h < 1$ and $1 < h < \sqrt{2}$. We identify the portions of the admissible region occupied by different JEF solutions and mark the staggered solutions with " $*$ " (see Sec. II D).

Admissible regions for $0 < \Lambda < 1$ [see in (a) and (b) of Fig. 1] are completely filled by the six JEF solutions: $(\mathrm{sn/cn})^*$, $(\mathrm{sndn/cn})^*$, sndn/cn, sn, 1/sn, and 1/cn (see Sec. II D).

In the range of $1 < \Lambda < 2$ [see in Fig. 1(d)] the solution sndn/cn disappears, while the remaining five solutions persist and, there appears a portion of the admissible region where we could not identify a JEF solution [marked with the question mark in (d)]. However, this solution can be easily obtained from the map Eq. (7) and one finds that the solution is unbounded.

The solution $(\mathrm{sn/cn})^*$ cannot be seen in (a)-(d) of Fig. 1 because it occupies the range of $-\infty < K < K^*$ with negative K^* falling outside the frames of the panels. In (a) and (b) of Fig. 1, the solution $(\mathrm{sndn/cn})^*$ takes a portion of K in between $(\mathrm{sn/cn})^*$ and sndn/cn solutions, but it falls out of the frames of these panels.

The only bounded solution in this case is the sn solution, which exists for $0 < K < 1/2$ when $h < 1$ and in a narrower range of K otherwise. For example, in panel Fig. 1(d), the sn solution exists for $0.425 < K < 1/2$. The kink solution, Eq. (38), corresponding to $K = 0$ and $-1 < \phi_0 < 1$, exists only for $h < 1$ (i.e. only for $0 < \Lambda < 1$).

Several static solutions generated by the map (7) for $h = 0.8$ [see panel (b) of Fig. 1] are presented in Fig. 2. In Fig. 2(a) we have the sndn/cn solution generated with $K = -0.25$, $\phi_0 = 0$; in Fig. 2(b), the sn solution close to the hyperbolic limit generated with $K = 10^{-8}$, $\phi_0 = 0$; in Fig. 2(c), the 1/sn solution close to the hyperbolic limit obtained for $K = 10^{-8}$, $\phi_0 = 1.1$; and in Fig. 2(d),

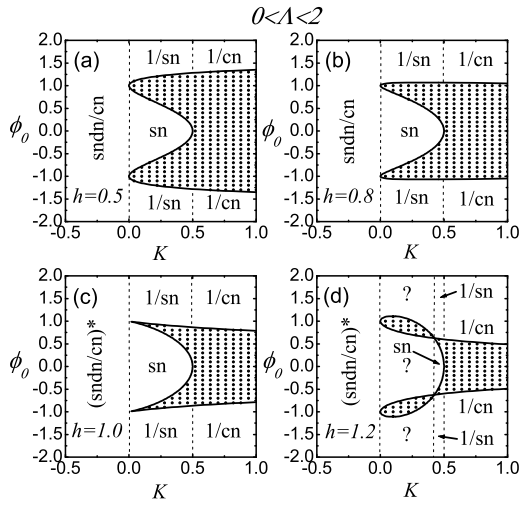

FIG. 1: Admissible and inadmissible (shaded) regions for the integration constants K and ϕ_0 for $\lambda = 1$ and different values of $h < \sqrt{2}$, indicated in each panel. The topology of the admissible regions is different for $h < 1$ and $1 < h < \sqrt{2}$. We identify the portions of the admissible region occupied by different JEF solutions and mark the staggered solutions with " $*$ " (see Sec. II D). The only bounded solution in this case is the sn solution which exists for $0 < K < 1/2$ when $h < 1$ and in a narrower range of K otherwise. For example, in panel (d), the sn solution exists for $0.425 < K < 1/2$. The kink solution, corresponding to $K = 0$ and $-1 < \phi_0 < 1$, exists only for $h < 1$. The solution $(\mathrm{sn/cn})^*$ cannot be seen in (a)-(d) because it occupies the range of $-\infty < K < \bar{K}$ with negative $\bar{K}$ being outside the frames of the panels. In (a) and (b), the solution $(\mathrm{sndn/cn})^*$ takes a portion of K in between $(\mathrm{sn/cn})^*$ and sndn/cn solutions, but it falls out of the frame of these panels. For the area marked with the question mark in (d) we could not identify a JEF solution. Several static solutions generated by the map of Eq. (7) for $h = 0.8$, panel (b), are presented in Fig. 2.

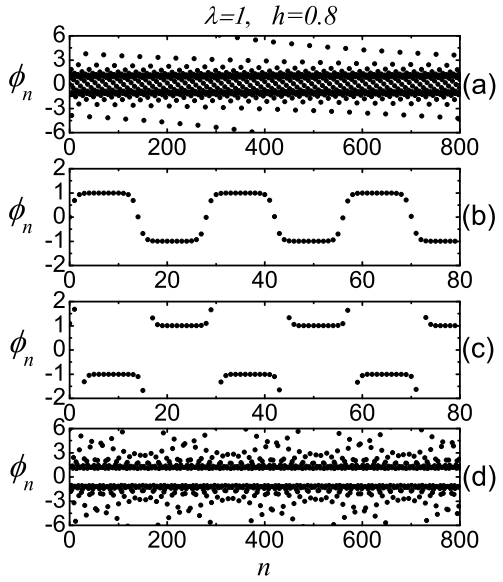

FIG. 2: Static solutions generated by the map Eq. (7) for $\lambda = 1$, $h = 0.8$ [see panel (b) of Fig. 1] for different values of the integration constants, K and ϕ_0. We have: (a) sndn/cn solution ($K = -0.25$, $\phi_0 = 0$); (b) sn solution close to the hyperbolic limit ($K = 10^{-8}$, $\phi_0 = 0$); (c) 1/sn solution close to the hyperbolic limit ($K = 10^{-8}$, $\phi_0 = 1.1$); and (d) 1/cn solution ($K = 0.75$, $\phi_0 = 1.25$). The only bounded solution is the sn solution shown in (b). Unbounded solutions have points with very large amplitudes falling outside the frames of the figures.

the 1/cn solution constructed for $K = 0.75$, $\phi_0 = 1.25$. The only bounded solution is the sn solution shown in Fig. 2(b), when it assumes the form of alternating kinks and anti-kinks. For unbounded solutions, the amplitudes of some points are very large and they fall outside the frames of the figures.

2. *Case of* $\Lambda > 2$

The inadmissible regions are shown by the shaded areas in Fig. 3 for different values of h, indicated in each panel. These are already quite different in structure from the inadmissible regions of Fig. 1; notice in particular the existence of such regions for positive K, near $\phi_0 = 0$, while in Fig. 1, admissible ϕ_0 exist for any K. Notice also a qualitative change of the border between admissible and inadmissible regions that takes place at $h = 2$ when the curvature of the border at the point $(K, \phi_0) = (1/2, 0)$ changes sign. One can see that, in this case, all static solutions are bounded. Admissible regions are completely filled by the three JEF solutions, cn, dn, and staggered dn, denoted as dn^* (see Sec. II D).

Examples of static solutions generated by the map of Eq. (7) for $\lambda = 1$, $h = 4$ [corresponds to panel (d) of Fig. 3] for different values of the integration constants, K and ϕ_0, are plotted in Fig. 4. The solutions are: (a) dn solution ($K = -0.05$, $\phi_0 = 1$); (b) zigzag solution, which is actually the dn^* solution in the limit of $m = 0$ ($K = 7/32$, $\phi_0 = \sqrt{3}/2$); (c) dn^* solution ($K = 0.26$, $\phi_0 = 1$); and (d) cn solution with $K(m) < \beta h < 2K(m)$ close to the hyperbolic limit, where it assumes the form of the chain of staggered pulses, Eq. (42), ($K = 1/2 + 10^{-12}$, $\phi_0 = 1$).

3. *Case of* $\Lambda < 0$

The inadmissible regions are shown by the shaded areas in Fig. 5 for (a) $h = 1.3$ and (b) $h = 4$. In this case, the topology does not change as one goes from small to

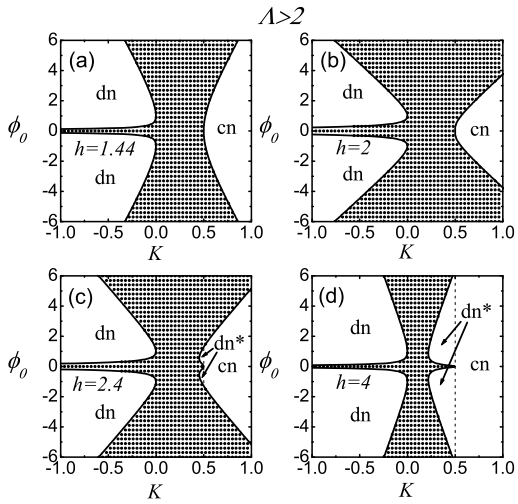

FIG. 3: Same as in Fig. 1 but for a regime of high discreteness, $h^2 > 2$. A qualitative change of the border between admissible and inadmissible regions takes place at $h = 2$ when the curvature of the border at the point $(K, \phi_0) = (1/2, 0)$ changes sign. All static solutions are bounded. Admissible regions are completely filled by the three JEF solutions, cn, dn, and staggered dn, denoted as dn* (see Sec. II D). Several static solutions generated by the map of Eq. (7) for $h = 4$, panel (d), are presented in Fig. 4.

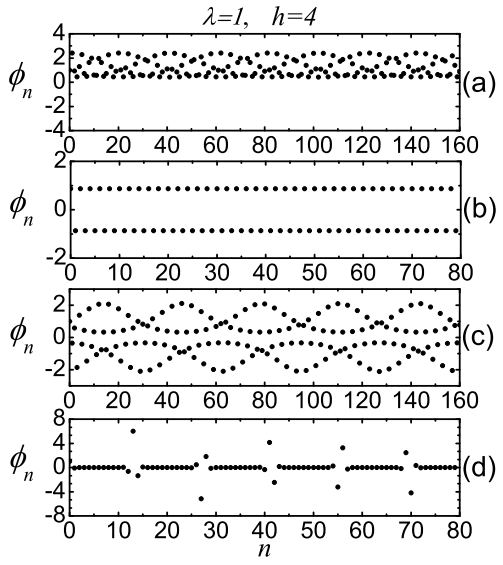

FIG. 4: Static solutions generated by the map of Eq. (7) for $\lambda = 1$, $h = 4$ [see panel (d) of Fig. 3] for different values of the integration constants, K and ϕ_0. All solutions are bounded. We have: (a) dn solution ($K = -0.05$, $\phi_0 = 1$); (b) zigzag solution, or the dn* solution in the limit of $m = 0$ ($K = 7/32$, $\phi_0 = \sqrt{3}/2$); (c) dn* solution ($K = 0.26$, $\phi_0 = 1$); and (d) the cn solution with $K(m) < \beta h < 2K(m)$ close to the hyperbolic limit, where it obtains the form of the chain of staggered pulses, Eq. (42), ($K = 1/2 + 10^{-12}$, $\phi_0 = 1$).

large h^2. All static solutions are bounded. The admissible regions are completely filled by the three JEF solutions, cn, dn, and staggered dn, marked as dn* (see Sec. II D).

Several static solutions generated by the map of Eq. (7) for $h = 1.3$ [refer to panel (a) of Fig. 5] are presented in Fig. 6. In (a), $K = -0.5 - 10^{-8}$, $\phi_0 = 1$; in (b), $K = -0.5 + 10^{-8}$, $\phi_0 = 1$; in (c), $K = -0.2$, $\phi_0 = 1$; and in (d), $K = 5.3$, $\phi_0 = 2$. The solutions in (a) and (b) are the cn and dn solutions close to the hyperbolic function limit, respectively. These solutions can be regarded as a lattice of pulses, Eq. (40). Solutions shown in (c) and (d) are dn and staggered dn solutions, respectively.

4. *Case* $\Lambda = 2$

In this case, the two-point map of Eq. (7) reduces to

$$\phi_n^2 \left(\phi_n^2 \phi_{n+1}^2 - 2\tilde{K} \phi_n \phi_{n+1} + \tilde{K} \right) = 0, \tag{16}$$

from which one has the trivial solution $\phi_n = 0$ and, for $\phi_n \neq 0$, one finds

$$\phi_{n+1} = \frac{1}{\phi_n} \left(\tilde{K} \pm \sqrt{\tilde{K}(\tilde{K} - 1)} \right). \tag{17}$$

This map defines the two-parameter space of solutions. Admissible regions of the (K, ϕ_0) plane correspond to $\tilde{K} \leq 0$ and $\tilde{K} \geq 1$. Due to the symmetry of Eq. (16), one can interchange ϕ_n and ϕ_{n+1} in Eq. (17). From the two different roots of Eq. (17) one must take ϕ_{n+1} such that the three point problem Eq. (1) is satisfied for ϕ_n; this would guarantee that one keeps moving along the same solution branch. It is sufficient to take ϕ_{n+1} different from ϕ_{n-1}, if the roots are different.

It is convenient to take the integration constant in the form

$$\tilde{K} = \frac{(1+a)^2}{4a}, \tag{18}$$

and consider $-1 \leq a \leq 1$ with $a \neq 0$. With this choice, for $-1 \leq a < 0$ we have $-\infty < \tilde{K} \leq 0$, while for $0 < a \leq 1$ we have $1 \leq \tilde{K} < +\infty$.

Taking for the initial value $\phi_0 = b$, where $b \neq 0$ is positive or negative real number, one can obtain from the map of Eq. (17) the following sequence, that satisfies both Eq. (1) and Eq. (16),

$$\phi_n : \left(..., b, \frac{(1+a)}{2b}, \frac{b}{a}, \frac{(1+a)a}{2b}, \frac{b}{a^2}, \frac{(1+a)a^2}{2b}, ... \right). \tag{19}$$

Note that for one of the bounds of the existence region, $\tilde{K} = 1$ ($a = 1$), solution Eq. (19) gives the following

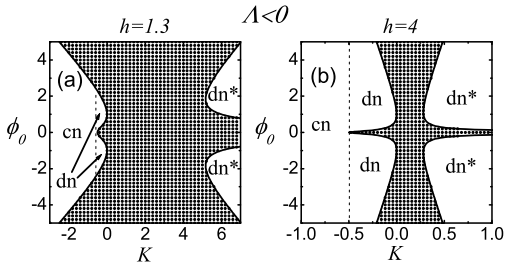

FIG. 5: Same as in Fig. 1 and Fig. 3 but for $\lambda = -1$. In this case, the topology does not change as one goes from small to large h^2. All static solutions are bounded. The admissible regions are completely filled by the three JEF solutions, cn, dn, and staggered dn (marked as dn*). Several static solutions generated by the map of Eq. (7) for $h = 1.3$, panel (a), are presented in Fig. 6.

.

family of two-site periodic solution

$$\phi_n : \left(..., b, \frac{1}{b}, b, \frac{1}{b}, ... \right). \tag{20}$$

On the other hand, the other bound of $\tilde{K} = 0$ ($a = -1$) gives from Eq. (19) the following four-site periodic solution

$$\phi_n : (..., b, 0, -b, 0, b, 0, ...). \tag{21}$$

It is worth pointing out that for the MC model (4) at $\Lambda = 2$, the two-point map has the form

$$(1 - \phi_n^2)[\phi_{n+1}^2(1 - \phi_n^2) - (1 - \phi_n^2) + \tilde{C}] = 0, \tag{22}$$

and, for $\phi_n \neq \pm 1$, we obtain

$$\phi_{n+1} = \pm\sqrt{1 - \frac{\tilde{C}}{1 - \phi_n^2}}. \tag{23}$$

Based on this expression, starting from any admissible value of ϕ_0 and for any chosen $\tilde{C}$, one can construct a solution iteratively. The topology of the admissible regions in this case is not as simple as in the case of model Eq. (1) at $\Lambda = 2$.

A four-site periodic solution for ϕ_n in this case is given by

$$\begin{aligned} &\phi_n : (..., a, b, -a, -b, a, b, -a, -b, a, ...), \\ &\tilde{C} = (1 - a^2)(1 - b^2), \end{aligned} \tag{24}$$

where a, b are any real numbers, positive or negative. In the special case of $\tilde{C} = 0$, apart from the above solution, another solution for the sequence ϕ_n is the arbitrary sequence of ± 1 with 0 put at random between -1 and $+1$ or between $+1$ and -1.

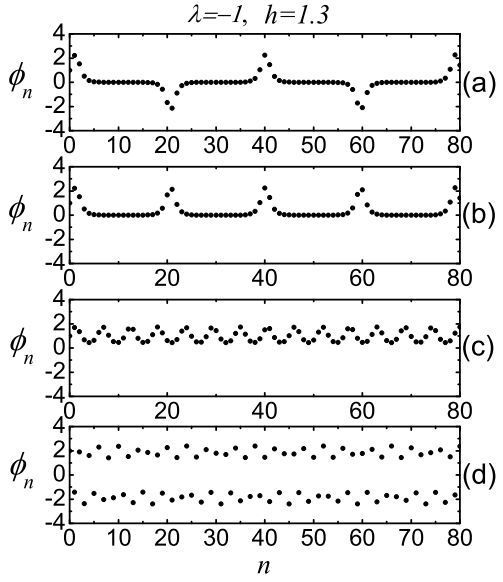

FIG. 6: Static solutions generated by the map of Eq. (7) for $\lambda = -1$, $h = 1.3$ [see panel (a) of Fig. 5] for different values of the integration constants, K and ϕ_0. In (a), $K = -0.5 - 10^{-8}$, $\phi_0 = 1$; in (b), $K = -0.5 + 10^{-8}$, $\phi_0 = 1$; in (c), $K = -0.2$, $\phi_0 = 1$; and in (d), $K = 5.3$, $\phi_0 = 2$. All the solutions are bounded. The solutions in (a) and (b) are the cn and dn solutions close to the hyperbolic function limit, respectively. The solution in (c) is the dn, while in (d) we show the staggered dn solution.

D. Static Jacobi elliptic function solutions

Motivated by the results of the previous section, let us now proceed to analytically identify several static JEF solutions to Eq. (1). The solutions can be derived from the three-point static problem of Eq. (1) with $\ddot{\phi}_n = 0$. In this case the use of the JEF identities listed in the Appendix II is particularly helpful. Alternatively, solutions can be derived from the DFI of Eq. (7). In this case, one also obtains the relation between the integration constant K and the parameters of the JEF solution thus establishing a link between the solutions obtained by two different approaches.

The results will be presented in the following way. We will first describe the general form of the derived JEF solutions, then give the parameters for the particular ones, and finally, we will characterize the solutions and describe the ranges of parameters where different solutions exist.

The general form of the solutions is

$$\begin{aligned} \phi_n &= \pm S A \mathrm{sn}^p(Z, m)\mathrm{cn}^q(Z, m)\mathrm{dn}^r(Z, m), \\ Z &= \beta h\,(n + x_0), \end{aligned} \tag{25}$$

where sn, cn, and dn are the Jacobi elliptic functions, $0 \leq m \leq 1$ is the modulus of JEF, A and β are the

parameters of the solution, and x_0 is the arbitrary initial position. For non-staggered solutions $S = 1$, while for staggered ones $S = (-1)^n$. Finally the integers p, q, r specify a particular form of the solution.

For the sake of brevity we introduce the following notations

$$s = \mathrm{sn}(\beta h, m), \quad c = \mathrm{cn}(\beta h, m), \quad d = \mathrm{dn}(\beta h, m). \tag{26}$$

Particular solutions have the following form and are characterized by the following parameters:

The sn solution, $(p, q, r) = (1, 0, 0)$,

$$A^2 = \frac{(2-\Lambda)ms^2}{\Lambda}, \quad A^2 = \frac{2ms^2cd}{\Lambda(1-ms^4)},$$
$$\tilde{K} = \frac{A^4}{m}, \quad S = 1. \tag{27}$$

The cn solution, $(p, q, r) = (0, 1, 0)$,

$$A^2 = \frac{(\Lambda-2)ms^2}{\Lambda d^2}, \quad A^2 = -\frac{2ms^2c}{\Lambda(d^2-ms^2c^2)},$$
$$\tilde{K} = -(1-m)\frac{A^4}{m}, \quad S = 1. \tag{28}$$

The dn solution, $(p, q, r) = (0, 0, 1)$,

$$A^2 = \frac{(\Lambda-2)s^2}{\Lambda c^2}, \quad A^2 = -\frac{2s^2d}{\Lambda(c^2-s^2d^2)},$$
$$\tilde{K} = (1-m)A^4, \quad S = 1. \tag{29}$$

The staggered sn* solution, $(p, q, r) = (1, 0, 0)$,

$$A^2 = \frac{(2-\Lambda)ms^2}{\Lambda}, \quad A^2 = -\frac{2ms^2cd}{\Lambda(1-ms^4)},$$
$$\tilde{K} = \frac{A^4}{m}, \quad S = (-1)^n. \tag{30}$$

The staggered cn* solution, $(p, q, r) = (0, 1, 0)$,

$$A^2 = \frac{(\Lambda-2)ms^2}{\Lambda d^2}, \quad A^2 = \frac{2ms^2c}{\Lambda(d^2-ms^2c^2)},$$
$$\tilde{K} = -(1-m)\frac{A^4}{m}, \quad S = (-1)^n. \tag{31}$$

The staggered dn* solution, $(p, q, r) = (0, 0, 1)$,

$$A^2 = \frac{(\Lambda-2)s^2}{\Lambda c^2}, \quad A^2 = \frac{2s^2d}{c^2-s^2d^2},$$
$$\tilde{K} = (1-m)A^4, \quad S = (-1)^n. \tag{32}$$

The 1/sn solution, $(p, q, r) = (-1, 0, 0)$,

$$A^2 = \frac{2s^2cd}{\Lambda(1-ms^4}, \quad A^2 = \frac{(2-\Lambda)s^2}{\Lambda},$$
$$\tilde{K} = A^4m, \quad S = 1. \tag{33}$$

The 1/cn solution, $(p, q, r) = (0, -1, 0)$,

$$A^2 = \frac{2(1-m)cs^2}{\Lambda(d^2-ms^2c^2}, \quad A^2 = \frac{(2-\Lambda)(1-m)s^2}{\Lambda d^2},$$
$$\tilde{K} = \frac{-mA^4}{1-m}, \quad S = 1. \tag{34}$$

The staggered (sn/cn)* solution, $(p, q, r) = (1, -1, 0)$,

$$A^2 = \frac{(1-m)(2-\Lambda)s^2}{\Lambda c^2}, \quad A^2 = -\frac{2(1-m)s^2d}{\Lambda(c^2-s^2d^2)},$$
$$\tilde{K} = \frac{A^4}{1-m}, \quad S = (-1)^n. \tag{35}$$

The sndn/cn solution, $(p, q, r) = (1, -1, 1)$,

$$A^2 = \frac{2s^2d^2(1-2ms^2+ms^4)}{\Lambda(c^4-s^4d^4)}, \quad A^2 = \frac{(2-\Lambda)s^2d^2}{\Lambda c^2},$$
$$\tilde{K} = A^4, \quad S = 1. \tag{36}$$

The staggered (sndn/cn)* solution, $(p, q, r) = (1, -1, 1)$,

$$A^2 = -\frac{2s^2d^2(1-2ms^2+ms^4)}{\Lambda(c^4-s^4d^4)}, \quad A^2 = \frac{(2-\Lambda)s^2d^2}{\Lambda c^2},$$
$$\tilde{K} = A^4, \quad S = (-1)^n. \tag{37}$$

It is worth making the following remarks:

To specify a particular solution, for given model parameters h^2 and λ, and for chosen m, one has to solve the first two equations entering Eqs. (27)-(37) in order to find the parameter β and then the amplitude A. If the equation for β has no solutions in the range of $0 < \beta h < 2K(m)$, this implies that for chosen h^2, λ, and m the corresponding JEF solution does not exist. Some of the roots for β can give imaginary amplitude A and we reject such solutions. On the other hand, if one or more roots for β in the range of $0 < \beta h < 2K(m)$ are found, then a JEF solution can be constructed for each root provided that the corresponding amplitude A is real. In Table I, for different JEF solutions, we summarize the location of roots for the parameter β, corresponding to real amplitude A and give the range of parameter Λ where the solutions exist. For comparison, similar results for bounded JEF solutions to the MC model of Eq. (4) are given in Table II.

In each of Eqs. (27)-(37) we give the corresponding expressions for $\tilde{K}$ in terms of the parameters of JEF solutions. These expressions link the JEF solutions to the nonlinear map Eq. (7), so that for each JEF solution one can find the corresponding portion of the (K, ϕ_0) plane. For example, the sn solution exists for $0 < \Lambda < 2$ (see Table I) and this case is shown in Fig. 1. Then, the sn solution having modulus m and amplitude A, in the (K, ϕ_0) plane will have abscissa K that can be found for given $\tilde{K}$ from Eq. (9) and the ordinate will vary in the range $-A \le \phi_0 \le A$. Considering different values of

TABLE I: Range of parameter Λ and location of the root for parameter β corresponding to real amplitude A for JEF solutions to Eq. (1)

Solution	Root for β within $0 < \beta h < K(m)$	Root for β within $K(m) < \beta h < 2K(m)$
sn, Eq. (27)	$0 < \Lambda < 2$	no solution
cn, Eq. (28)	$\Lambda < 0$	$\Lambda > 2$
dn, Eq. (29)	$\Lambda < 0$	$\Lambda > 2$
sn*, Eq. (30)	no solution	$0 < \Lambda < 2$
cn*, Eq. (31)	$\Lambda > 2$	$\Lambda < 0$
dn*, Eq. (32)	$\Lambda > 2$	$\Lambda < 0$
1/sn, Eq. (33)	$0 < \Lambda < 2$	no solution
1/cn, Eq. (34)	$0 < \Lambda < 2$	no solution
(sn/cn)*, Eq. (35)	$0 < \Lambda < 2$	$0 < \Lambda < 2$
sndn/cn, Eq. (36)	$0 < \Lambda < 1$	$0 < \Lambda < 1$
(sndn/cn)*, Eq. (37)	$0 < \Lambda < 2$	$0 < \Lambda < 2$

TABLE II: Same as in Table I but for the bounded JEF solutions to the MC model Eq. (4)

Solution	Root for β within $0 < \beta h < K(m)$	Root for β within $K(m) < \beta h < 2K(m)$
sn	$0 < \Lambda < 2$	$\Lambda > 2$
cn	$\Lambda < 0$	no solution
dn	$\Lambda < 0$	no solution
sn*	$\Lambda > 2$	$0 < \Lambda < 2$
cn*	no solution	$\Lambda < 0$
dn*	no solution	$\Lambda < 0$

$0 \le m \le 1$, one can see that the sn solution occupies the portions marked with "sn" in Fig. 1.

The solutions presented by Eqs. (27)-(32) are bounded while the other solutions are unbounded.

The sn solution and its staggered form sn* are in fact equivalent in the sense that any sequence of ϕ_n produced by one of them can also be produced by the other. As a result, sn and sn* solutions occupy the same portion of the (K, ϕ_0) plane (see Fig. 1). The same can be said about the pair of solutions cn and cn*. However, the dn solution is essentially different from its staggered form, dn*, and also the sndn/cn solution is essentially different from its staggered form, (sndn/cn)*.

E. Hyperbolic function static solutions

In the limit of $m \to 1$ the sn solution given by Eqs. (25) and (27) reduces to the kink (antikink) solution

$$\phi_n = \pm \tanh[\beta h(n + x_0)], \tag{38}$$

where x_0 is an arbitrary shift, β satisfies

$$\tanh^2(\beta h) = \frac{\Lambda}{2 - \Lambda}, \tag{39}$$

and $\tilde{K} = 1$, i.e., $K = 0$.

TABLE III: Range of parameter Λ for hyperbolic solutions to Eq. (1)

Solution	Exists for
Kink, Eq. (38)	$0 < \Lambda < 1$
Pulse, Eq. (40)	$\Lambda < 0$
Staggered kink	no solution
Staggered pulse, Eq. (42)	$\Lambda > 4$

TABLE IV: Same as in Table III but for MC model Eq. (4)

Solution	Exists for
Kink	$0 < \Lambda < 2$
Pulse	$\Lambda < 0$
Staggered kink	$\Lambda > 2$
Staggered pulse	no solution

In the limit of $m \to 1$, both the cn solution and the dn solution with parameters given by Eq. (28) and Eq. (29), respectively, reduce to the same pulse solution

$$\phi_n = \pm A \mathrm{sech}[\beta h(n + x_0)], \tag{40}$$

where x_0 is an arbitrary shift, β and A can be found from

$$\begin{aligned} \cosh(\beta h) &= \frac{2 - \Lambda}{2}, \\ \Lambda A^2 &= (\Lambda - 2)\sinh^2(\beta h), \end{aligned} \tag{41}$$

and $\tilde{K} = 0$, i.e., for $\lambda = -1$, $K = -1/2$.

We now turn to the case of staggered hyperbolic function solutions. It is easily checked from Eq. (30) that the TI model of Eq. (1) does not support the staggered kink solution (even though it supports the sn* solution). However, it supports the staggered pulse solution

$$\phi_n = \pm(-1)^n A \mathrm{sech}[\beta h(n + x_0)], \tag{42}$$

where x_0 is an arbitrary shift, β and A can be found from

$$\begin{aligned} \cosh(\beta h) &= \frac{\Lambda - 2}{2}, \\ \Lambda A^2 &= (\Lambda - 2)\sinh^2(\beta h). \end{aligned} \tag{43}$$

and $\tilde{K} = 0$, i.e., for $\lambda = 1$, $K = 1/2$.

In Table III we present the ranges of model parameter Λ where the hyperbolic function solutions exist in the model of Eq. (1) and, for comparison, in Table IV we give similar results for the MC model of Eq. (4).

III. LINEAR STABILITY AND DYNAMICS FOR BOUNDED SOLUTIONS FOR $h^2 < 2$

A. Linear stability

Introducing the ansatz $\phi_n(t) = \phi_n^0 + \varepsilon_n(t)$ (where ϕ_n^0 is an equilibrium solution and $\varepsilon_n(t)$ is a small perturbation), we linearize Eq. (1) with respect to ε_n, in order

to examine the linear stability of the above-established solutions. In this way, we obtain the following equation:

$$\ddot{\varepsilon}_n = \frac{1}{h^2}(\varepsilon_{n-1} - 2\varepsilon_n + \varepsilon_{n+1}) + \lambda\varepsilon_n$$
$$-\lambda\phi_n^0\phi_{n+1}^0\varepsilon_{n-1} - \lambda\phi_{n-1}^0\phi_{n+1}^0\varepsilon_n - \lambda\phi_{n-1}^0\phi_n^0\varepsilon_{n+1}. \quad (44)$$

For the small-amplitude phonons, $\varepsilon_n = \exp(ikn + i\omega t)$, with frequency ω and wave number k, Eq. (44) is reduced to the following dispersion relation:

$$\omega^2 = \frac{4}{h^2}\sin^2\left(\frac{k}{2}\right) - \lambda + \lambda\phi_{n-1}^0\phi_{n+1}^0$$
$$+\lambda\phi_n^0\phi_{n+1}^0 e^{-ik} + \lambda\phi_{n-1}^0\phi_n^0 e^{ik}, \quad (45)$$

where it is assumed that ϕ_n^0 is a uniform steady state solution (or a zigzag solution; see below). The corresponding eigenvalue problem has a non-symmetric matrix. This fact is a manifestation of the non-Hamiltonian nature of Eq. (1).

Stability of vacuum solutions. From Eq. (45), the spectrum of the vacuum solution $\phi_n^0 = \pm 1$ (at $\lambda = 1$) is

$$\omega^2 = 2 + \frac{4}{h^2}(1 - h^2)\sin^2\left(\frac{k}{2}\right). \quad (46)$$

This solution is stable for $h^2 \leq 2$.

The spectrum of the vacuum solution $\phi_n^0 = 0$ (at $\lambda = -1$) is

$$\omega^2 = 1 + \frac{4}{h^2}\sin^2\left(\frac{k}{2}\right), \quad (47)$$

and this solution is stable for any value of h^2.

Stability of kink solution. As it can be seen from Eq. (39), the kink solution Eq. (38) exists only for $\lambda = 1$ and $h^2 < 1$. The spectrum of lattice with a kink as a function of lattice spacing h is shown in Fig. 7 for the on-site kink, $x_0 = 0$ (open circles), and inter-site kink, $x_0 = h/2$ (dots). The corresponding kink profiles are shown in the inset for $h = 0.8$. Two solid lines show the borders of the spectrum of vacuum, Eq. (46). The kink possesses the translational internal mode with $\omega^2 = 0$ and also the localized modes with frequencies below the phonon band and a localized mode with frequency above the phonon band. The kink is stable in the whole range of existence, $h^2 < 1$. Notice also that as the continuum limit $h \to 0$ is approached, a number of internal modes that exist for larger h disappear into the phonon band of Eq. (46); the only internal mode that persists with $\omega \to \sqrt{3}$, as $h \to 0$ is the well-known continuum ϕ^4 model internal mode (see e.g. [6] and references therein).

Instability of the zigzag solution. In the sinusoidal function limit ($m = 0$), the staggered dn solution defined by Eq. (25) and Eq. (32) reduces to the zigzag solution

$$\phi_n = (-1)^n A, \qquad A^2 = \frac{\Lambda - 4}{\Lambda}. \quad (48)$$

Note that this solution is valid if $\Lambda > 4$ or if $\Lambda < 0$. Substituting this solution into Eq. (45) we obtain the dispersion relation $\omega^2 h^2 = 4 - 2\Lambda + 4(\Lambda - 3)\sin^2(k/2)$. One can see that the spectrum of the zigzag solution always contains imaginary frequencies in both cases, $\Lambda > 4$ and $\Lambda < 0$, and thus, the solution is always unstable.

Stability of solutions at $\Lambda = 2$. In this case (see Sec. II C 4), we have two bounded solutions, Eq. (20) and Eq. (21). For the two-periodic solution Eq. (20), the vibrational spectrum has two branches, $(h^2\omega^2)_{1,2} = a^2 + 1/a^2 \pm \sqrt{(a^2 + 1/a^2)^2 - 2 + 2\cos k}$. Since $a^2 + 1/a^2 \geq 2$ for any a, ω^2 is always non-negative and the solution is always stable. Numerically we found that the four-periodic solution Eq. (21) is always unstable. This can be justified by introducing a small deviation ε into the position of a particle with $\phi = 0$, while keeping all other particles in their equilibrium positions. The right-hand side of Eq. (1) gives the force acting on the particle equal to $2\varepsilon a^2$. Since the sign of the force coincides with the sign of the displacement, the solution is indeed unstable with respect to the considered perturbation.

For the MC model Eq. (4) in the case of $\Lambda = 2$, we found that the solutions $..., -1, 1, -1, 1, ...$ and $..., -1, 0, 1, -1, 0, 1, ...$ are unstable. This can be checked by introducing a small displacement into position of a particle with $\phi = 1$, keeping other particles at their equilibrium positions. We then calculate the increment of force acting on this particle and find that it has the same sign as the displacement, which proves the instability with respect to this type of perturbation.

Calculating the increment of force acting on a particle with unperturbed amplitude $\phi = 1$ in response to a small displacement ε of this particle, we found that it has the same sign as the displacement. Thus, these two solutions are unstable and this fact was also confirmed numerically.

Stability of other solutions. We also examined numerically the stability of other ones among the above-found solutions. We studied bounded, periodic Jacobi elliptic function solutions depicted in Fig. 1 and Fig. 5(a), i.e., the sn, cn, dn, and staggered dn solutions. The length of the chain was compatible with the period of the solution and it contained a few periods. The eigenvalue problem obtained by replacing the left-hand side of Eq. (44) with $-\omega^2\varepsilon_n$ was solved numerically under periodic boundary conditions. The sn, cn, dn, staggered dn, and the pulse solutions were found to be generically unstable, i.e., having negative eigenfrequencies ω^2 in their numerical spectra.

It is important to note that all the solutions possess the zero-frequency translational eigenmode due to the TI nature of the lattice of Eq. (1). As an overview of the results of the stability analysis, we find that, among the bounded solutions, only the kink solution, the vacuum solutions, and the solution of Eq. (20) ($\Lambda = 2$ case) can be stable. Note that exactly the same conclusion was also reached in the case of the MC model [9] in case $\Lambda \neq 2$.

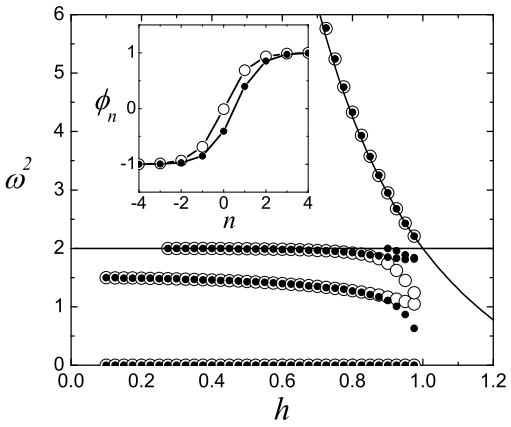

FIG. 7: Frequencies of the kink's internal modes for different magnitudes of the discreteness parameter h. Results for the on-site (circles) and inter-site (dots) kinks. The corresponding kink profiles are shown in the inset for $h = 0.8$. Two solid lines show the borders of the spectrum of vacuum, Eq. (46). The kink possesses the translational internal mode with $\omega^2 = 0$ and also the localized modes with frequencies below the phonon band and a localized mode with the frequency above the phonon band. The kink is stable in the whole range of its existence, $h^2 < 1$.

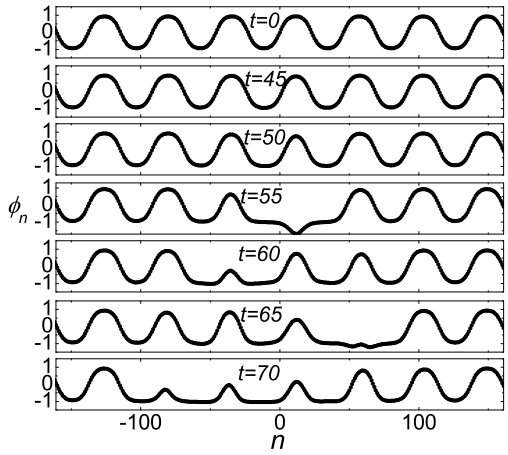

FIG. 8: Time evolution of the sn solution perturbed at $t = 0$ by shifting the position of $n = 0$ particle by -10^{-2}. The model parameters are $F = \lambda = 1$, $h = 0.25$ and the parameters of the sn solution are $m \simeq 0.777$, $x_0 = 0$.

B. Dynamics of unstable solutions

In the figures 8-10 we give examples of the dynamical behavior of the unstable static solutions perturbed at $t = 0$ by adding a small displacement to the 0-th particle.

In Fig. 8 the sn solution was perturbed at $t = 0$ by shifting the position of $n = 0$ particle by -10^{-2}. The model parameters are chosen as $\lambda = 1$, $h = 0.25$ and the parameters of the sn solution are $m \simeq 0.777$, $x_0 = 0$. Up to the time $t \approx 45$ the long-wave mode of deviation from equilibrium, growing exponentially with time, remains indistinguishable in the scale of the figure. After that, the sn solution gradually slides down into the potential well at $\phi = -1$ and a set of breather-like oscillating pulses is formed. The oscillations are accompanied by phonon radiation and their amplitude decreases in time. The instability picture presented in Fig. 8 can also be interpreted in terms of the kink-antikink interactions. Such interactions are attractive and the chain of mutually attractive quasi-particles, as it is well-known, is unstable and cannot remain equally spaced in the presence of small perturbations.

Similar behavior is demonstrated by the unstable pulse perturbed at $t = 0$ by shifting the position of the $n = 0$ particle by -10^{-4} (see Fig. 9). The pulse slides down into the potential well at $\phi = 0$ and oscillates by radiating energy. The pulse is shown at the moment of maximum displacement of the central particle. The period of oscillation of the pulse is roughly equal to 7. The model parameters are $\lambda = -1$, $h = 0.25$ and the pulse is placed at $x_0 = 0$. We note in passing that the instability of the single pulse has been demonstrated quite generally for discrete TI settings in the case of the ϕ^4 equation in [9]; on the basis of that proof, we expect the individual pulses (as well as solutions consisting of concatenations of such pulses) to be unstable in the present model as well.

In Fig. 10 the time evolution of the unstable dn solution perturbed at $t = 0$ by shifting the position of the $n = 0$ particle by -10^{-4} is presented. The model parameters are $\lambda = -1$, $h = 0.25$ and the parameters of the dn solution are $m = 0.3$, $x_0 = 0$. The dn solution has particles situated near the top of the potential barrier at $\phi = 1$ and, being perturbed as described above, the particles, one after another, slide down into the potential well at $\phi = 0$ and oscillate near the potential well.

Note that the perturbation of the opposite sign (outward of the potential well at $\phi = 0$) would cause the divergence of the pulse and the dn solutions shown in the top panels of Fig. 9 and Fig. 10, respectively. We note that qualitatively similar behavior was also observed in the case of the MC model [9].

IV. DISCUSSION AND CONCLUSIONS

For a non-standard, translationally invariant discrete lattice, namely the discretization of the ϕ^4 model of Eq. (1), we have reported a number of important developments. We have explicitly identified the momentum conservation law given by Eq. (5), produced a set of static solutions in terms of the Jacobi elliptic functions, including the staggered ones, see Sec. II D and their hyperbolic

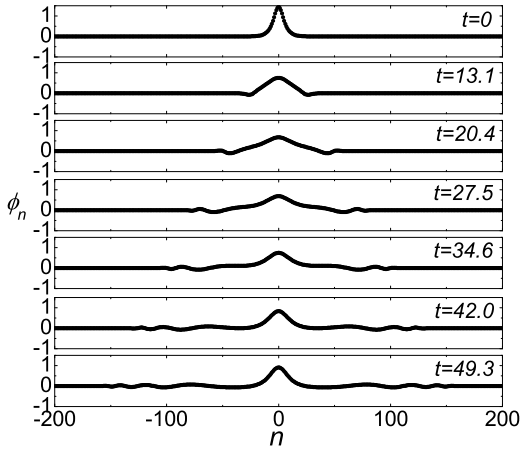

FIG. 9: Time evolution of the pulse solution perturbed at $t = 0$ by shifting the position of $n = 0$ particle by -10^{-4}. The pulse is shown at the moment of maximum displacement of the central particle. The period of oscillation of the pulse is roughly equal to 7. The model parameters are $F = \lambda = -1$, $h = 0.25$ and the pulse is placed at $x_0 = 0$.

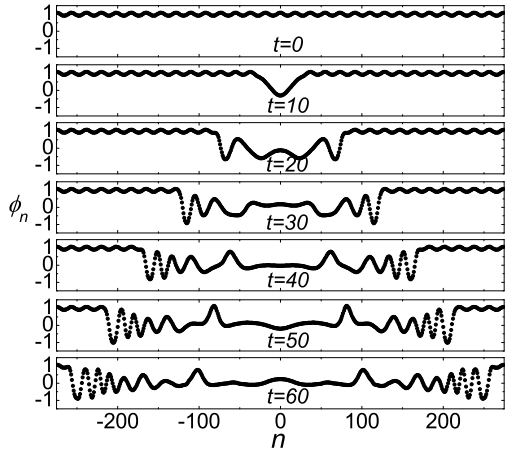

FIG. 10: Time evolution of the dn solution perturbed at $t = 0$ by shifting the position of the $n = 0$ particle by -10^{-4}. The model parameters are $F = \lambda = -1$, $h = 0.25$ and the parameters of the dn solution are $m = 0.3$, $x_0 = 0$.

limit. We have fully analysed the existence of such solutions, as well as detailed their linear stability. In Appendix I, we have demonstrated how, using a JEF solution of Eq. (1), one can construct the nonlinear map (or DFI) of Eq. (7). Importantly, we have proposed this as an illustrative example of how to formulate the discrete first integral approach, how to link it to the Jacobi elliptic function solutions, how to construct the complete space of solutions of the static problem, and identify the associated conservation law for such discrete, translationally invariant models.

An important feature of our approach is that from the nonlinear map Eq. (7), *any* static solution of Eq. (1) can be obtained recurrently, solving at each step a simple algebraic problem, in our case, a quadratic equation. Admissible values of the integration constants K and ϕ_0 have been plotted for positive and negative λ and for different values of the discreteness parameter h^2, see Figs. 1, 3, and 5. Any point inside the admissible region corresponds to the static solutions of Eq. (1).

We expect that the results presented herein for the discrete ϕ^4 equation can be applied to analogous discrete nonlinear Schrödinger type equations, similarly to what was discussed in the recent works [12, 19, 20, 23]. Another very natural extension of the present approach, detailing how to obtain an analytical handle on solutions of such translationally invariant models, would be to consider higher dimensional settings. Very little is known even in 2+1-dimensional spatially discrete models about analytical solutions, hence such investigations would be a particularly interesting next step in this direction of research.

Appendix I

In this Appendix we show how the two-point maps can be constructed directly from the known exact solutions. For example, for the tanh solution Eq. (38) one can find ϕ_{n-1} or ϕ_{n+1} using the identity $\tanh(x+y) = (\tanh x + \tanh y)/(1 + \tanh x \tanh y)$ and then, making use of Eq. (38) and Eq. (39) write down the two-point map that generates the tanh solution

$$\phi_{n\pm1} = \frac{\phi_n \pm T}{1 \pm T\phi_n}, \quad T = \sqrt{\frac{\Lambda}{2-\Lambda}}. \tag{49}$$

This map does not involve the integration constant because for the tanh solution we have already set $m = 1$. The initial value can be chosen arbitrarily from the range $-1 < \phi_0 < 1$.

Similarly, for the sn solution, Eq. (25) and Eq. (27), using the formula for $\mathrm{sn}(x+y)$, we can write

$$\phi_{n\pm1} = A\frac{cdS \pm sCD}{1 - ms^2S^2}, \tag{50}$$

where we have denoted

$$\begin{aligned} S &= \mathrm{sn}[\beta h(n+x_0), m], \\ C &= \mathrm{cn}[\beta h(n+x_0), m], \\ D &= \mathrm{dn}[\beta h(n+x_0), m], \end{aligned} \tag{51}$$

and also used the notations of Eq. (26). According to Eq. (27) we have $\phi_n = AS$ and, using the identity for the Jacobi elliptic functions $C^2D^2 = 1 - (1+m)S^2 + mS^4$,

we rewrite Eq. (50) in the form of the two-point map

$$\phi_{n\pm1} = \frac{Acd\phi_n \pm s\sqrt{A^4 - (1+m)A^2\phi_n^2 + m\phi_n^4}}{A - ms^2\phi_n^2/A}. \quad (52)$$

The integration constant here is $0 \le m \le 1$. As soon as m is specified, one can find β and A from Eq. (27) and then s, c, d from Eq. (26), thus defining the map Eq. (52). The corresponding sn solution can be constructed by iterating Eq. (52) starting from any initial value taken from $-A \le \phi_0 \le A$.

By analogy, two-point maps can be constructed for any solution given in Sec. II D and Sec. II E. However, each of the maps constructed in this way is parameterized by the modulus m and can be applied only to the corresponding solution. In our case, it is possible to substitute m with a universal integration constant so that the resulting two-point map can generate all static solutions of Eq. (1). The universal integration constant can be taken, e.g., as

$$K = \frac{\lambda}{2}\left(1 - \frac{A^4}{m}\right), \quad (53)$$

then we have

$$\tilde{K} = 1 - \frac{2K}{\lambda} = \frac{A^4}{m}. \quad (54)$$

From Eq. (27) one can derive

$$cd = Z, \qquad \frac{(1+m)\,A^2}{m} = X, \quad (55)$$

where Z and X are given by Eq. (10) and Eq. (11), respectively. With the help of Eq. (27) and Eqs. (53)-(55) we transform Eq. (52) to the form of Eq. (7) which does not include explicitly the parameters of the sn solution.

Appendix II

In the derivation of the Jacobi elliptic function solutions presented in Sec. II D, the following identities for Jacobi elliptic functions have been used [25]

$$\begin{aligned} &m\mathrm{sn}(x+a)\mathrm{sn}(x)\mathrm{sn}(x-a) \\ &= \mathrm{ns}(a)\mathrm{ns}(2a)[\mathrm{sn}(x+a) + \mathrm{sn}(x-a)] \\ &\quad -\mathrm{ns}^2(a)\mathrm{sn}(x), \end{aligned} \quad (56)$$

$$\begin{aligned} &m\mathrm{cn}(x+a)\mathrm{cn}(x)\mathrm{cn}(x-a) \\ &= -\mathrm{ds}(a)\mathrm{ds}(2a)[\mathrm{cn}(x+a) + \mathrm{cn}(x-a)] \\ &\quad +\mathrm{ds}^2(a)\mathrm{cn}(x), \end{aligned} \quad (57)$$

$$\begin{aligned} &m\mathrm{dn}(x+a)\mathrm{dn}(x)\mathrm{dn}(x-a) \\ &= -\mathrm{cs}(a)\mathrm{cs}(2a)[\mathrm{dn}(x+a) + \mathrm{dn}(x-a)] \\ &\quad +\mathrm{cs}^2(a)\mathrm{dn}(x). \end{aligned} \quad (58)$$

On the other hand, in the case of the MC model [9], the following identities are required for deriving the JEF solutions [25]

$$\begin{aligned} &m\mathrm{sn}^2(x)[\mathrm{sn}(x+a) + \mathrm{sn}(x-a)] \\ &= \mathrm{ns}^2(a)[\mathrm{sn}(x+a) + \mathrm{sn}(x-a)] \\ &\quad -2\mathrm{cs}(a)\mathrm{ds}(a)\mathrm{sn}(x), \end{aligned} \quad (59)$$

$$\begin{aligned} &m\mathrm{cn}^2(x)[\mathrm{cn}(x+a) + \mathrm{cn}(x-a)] \\ &= -\mathrm{ds}^2(a)[\mathrm{cn}(x+a) + \mathrm{cn}(x-a)] \\ &\quad +2\mathrm{cs}(a)\mathrm{ns}(a)\mathrm{cn}(x), \end{aligned} \quad (60)$$

$$\begin{aligned} &m\mathrm{dn}^2(x)[\mathrm{dn}(x+a) + \mathrm{dn}(x-a)] \\ &= -\mathrm{cs}^2(a)[\mathrm{dn}(x+a) + \mathrm{dn}(x-a)] \\ &\quad +2\mathrm{ds}(a)\mathrm{ns}(a)\mathrm{dn}(x). \end{aligned} \quad (61)$$

Acknowledgements

PGK gratefully acknowledges support from NSF-DMS-0204585, NSF-DMS-0505663 and NSF-CAREER. This work was supported in part by the U.S. Department of Energy.

[1] M. Toda, *Theory of Nonlinear Lattices* (Springer-Verlag, Berlin, 1981).

[2] O.M. Braun and Yu.S. Kivshar, *The Frenkel-Kontorova Model: Concepts, Methods and Applications* (Springer-Verlag, Berlin, 2004).

[3] F. R. N. Nabarro, *Theory of Crystal Dislocations* (Clarendon Press, Oxford, 1967).

[4] T. R. O. Melvin, A. R. Champneys, P. G. Kevrekidis, and J. Cuevas Phys. Rev. Lett. **97**, 124101 (2006)

[5] Oliver Morsch and Markus Oberthaler Rev. Mod. Phys.

78, 179 (2006)
[6] P. G. Kevrekidis, Physica D **183**, 68 (2003).
[7] J. M. Speight, and R. S. Ward, Nonlinearity **7**, 475 (1994); J. M. Speight, Nonlinearity **10**, 1615 (1997); J. M. Speight, Nonlinearity **12**, 1373 (1999).
[8] F. Cooper, A. Khare, B. Mihaila, and A. Saxena, Phys. Rev. E **72**, 36605 (2005).
[9] S. V. Dmitriev, P. G. Kevrekidis, N. Yoshikawa, and D. J. Frantzeskakis, Phys. Rev. E **74**, 046609 (2006).
[10] J. M. Speight and Y. Zolotaryuk, Nonlinearity **19**, 1365 (2006).
[11] O.F. Oxtoby, D.E. Pelinovsky and I.V. Barashenkov, Nonlinearity **19**, 217 (2006).
[12] S.V. Dmitriev, P.G. Kevrekidis, N. Yoshikawa and D. J. Frantzeskakis, J. Phys. A **40**, 1727 (2007).
[13] M. J. Ablowitz and J. F. Ladik, J. Math. Phys. **16**, 598 (1975); M. J. Ablowitz and J. F. Ladik, J. Math. Phys. **17**, 1011 (1976).
[14] S. J. Orfanidis, Phys. Rev. D **18**, 3828 (1978).
[15] G.R.W. Quispel, J.A.G. Roberts and C.J. Thompson, Physica D **34**, 183 (1989).
[16] S. V. Dmitriev, P. G. Kevrekidis, and N. Yoshikawa, J. Phys. A **39**, 7217 (2006).
[17] S. V. Dmitriev, P. G. Kevrekidis, and N. Yoshikawa, J. Phys. A **38**, 7617 (2005).
[18] I. V. Barashenkov, O. F. Oxtoby, and D. E. Pelinovsky, Phys. Rev. E **72**, 35602R (2005).
[19] P. G. Kevrekidis, S. V. Dmitriev, and A. A. Sukhorukov, *Math. Comput. Simul.* doi:10.1016/j.matcom.2006.10.014.
[20] S.V. Dmitriev, P.G. Kevrekidis, A.A. Sukhorukov, N. Yoshikawa and S. Takeno, Phys. Lett. A **356**, 324 (2006) (see also nlin.PS/0603047, with corrected misprints).
[21] A. Khare, K. Rasmussen, M.R. Samuelsen and A. Saxena, J. Phys. A **38**, 807-8 (2005).
[22] A. Khare, K. Rasmussen, M. Salerno, M.R. Samuelsen and A. Saxena, Phys. Rev. E **74**, 016607-11 (2006).
[23] D. E. Pelinovsky, Nonlinearity **19**, 2695 (2006).
[24] *Handbook of mathematical functions*, edited by M. Abramowitz and I. A. Stegun (U. S. GPO, Washington, D.C., 1964).
[25] A. Khare and U.P. Sukhatme, J. Math. Phys. **43**, 3798 (2002); A. Khare, A. Lakshminarayan and U.P. Sukhatme, J. math. Phys. **44**, 1822 (2003); ibid, Pramana (Journal of Physics) **62**, 1201 (2004), math-ph/0306028.